Lack of universality in decaying magnetohydrodynamic turbulence

E. Lee,[1,2] M. E. Brachet,[1,3] A. Pouquet,[1] P. D. Mininni,[1,4] and D. Rosenberg[1]

[1]*Geophysical Turbulence Program, National Center for Atmospheric Research, P.O. Box 3000, Boulder, Colorado 80307-3000, USA*

[2]*Centrum voor Plasma-Astrofysica, Departement Wiskunde, Katholieke Universiteit Leuven, Celestijnenlaan 200B, B-3001 Leuven, Belgium*

[3]*École Normale Supérieure, 24 rue Lhomond, 75005 Paris, France*

[4]*Departamento de Física, Facultad de Ciencias Exactas y Naturales, Universidad de Buenos Aires, Ciudad Universitaria,*

1428 Buenos Aires, Argentina

Using computations of three-dimensional magnetohydrodynamic (MHD) turbulence with a Taylor-Green flow, whose inherent time-independent symmetries are implemented numerically, and in the absence of either a forcing function or an imposed uniform magnetic field, we show that three different inertial ranges for the energy spectrum may emerge for three different initial magnetic fields, the selecting parameter being the ratio of nonlinear eddy to Alfvén time. Equivalent computational grids range from 128^3 to 2048^3 points with a unit magnetic Prandtl number and a Taylor Reynolds number of up to 1500 at the peak of dissipation. We also show a convergence of our results with Reynolds number. Our study is consistent with previous findings of a variety of energy spectra in MHD turbulence by studies performed in the presence of both a forcing term with a given correlation time and a strong, uniform magnetic field. However, in contrast to the previous studies, here the ratio of characteristic time scales can only be ascribed to the intrinsic nonlinear dynamics of the paradigmatic flows under study.

PACS number(s): 47.27.−i, 47.65.−d

I. INTRODUCTION

Turbulence forms the backbone of many natural phenomena in the atmosphere and ocean, as well as in astrophysical flows. In the latter, it is often accompanied by the coupling of vortices and current structures. For incompressible neutral fluids, under the assumption of a high Reynolds number (and therefore a long dissipation time), as is the case for many geophysical flows, the relevant time scale for the problem is the nonlinear eddy-turnover time. For such flows, the phenomenology developed by Kolmogorov in 1941 (hereafter referred to as "K41") [1], predicting a kinetic-energy spectrum $E_{\mathrm{K41}}^V(k) \sim k^{-5/3}$, represents a good first approach even if corrections to this phenomenology for higher-order statistics are known to exist due to the breakdown of the self-similarity represented by a simple power-law energy spectrum. When electromagnetic forces are introduced, other time scales can arise, such as the Alfvén time, associated with the propagation of transverse waves along magnetic field lines. K41 phenomenology may still apply, but one must also consider the role of Alfvén waves in producing a different power law for the total-energy spectrum, as illustrated independently by Iroshnikov and Kraichnan (hereafter, "IK") [2]: $E_{\mathrm{IK}}^T(k) \sim k^{-3/2}$.

Isotropy is assumed by both K41 and IK, but it is not necessarily achieved. In neutral flows, if the anisotropy of the small scales, in the form of elongated vortex filaments, occurs locally in space, isotropy may be recovered overall because the filaments are randomly oriented and the vorticity spectrum $k^2 E^V(k)$, which peaks in the small scales, contributes little to the large-scale energy spectrum. In contrast, the anisotropy of magnetohydrodynamics (MHD) originates from a large-scale magnetic field, which can be dominant energetically and relevant at all scales. Studies of anisotropic MHD date back to the mid-1950s for liquid metals at low

magnetic Reynolds number [3] (see also [4]) and a bit later for fully developed MHD turbulence [5,6]. More recently, a wealth of new studies on MHD turbulence has been made possible [7–9] in part by the revival of weak turbulence theory (e.g., [10] for MHD), the availability of more detailed observations [11,12], and improved resolution in numerical simulations [13–17].

From the theoretical point of view, the presence of a strong background magnetic field $\mathbf{B}_0$ allows for the existence of a small parameter characterizing the ratio of velocity and magnetic field fluctuations to $|\mathbf{B}_0|$, enabling an analytical solution via the weak turbulence (hereafter, "WT") approach. In contrast to the K41 and IK spectra, the WT energy spectrum is anisotropic: $E_{\mathrm{WT}}(k_\perp, k_\parallel) \sim k_\perp^{-2}$, where perpendicular and parallel are relative to the direction of $\mathbf{B}_0$; there is, in fact, no prescribed transfer in $k_\parallel$ at lowest order. Note that, interestingly, the IK phenomenology is compatible with weak turbulence in the isotropic limit, giving it a stronger theoretical footing. Other phenomenological approaches hypothesize that even with a strong background field $\mathbf{B}_0$ making the flow highly anisotropic, an "anisotropic Kolmogorov" scaling of the energy spectrum is possible by way of a dynamical effect that makes the two characteristic times of the problem (the Alfvén time and the eddy-turnover time) equal at all scales [18]. In fact, when this hypothesis is relaxed to a constant ratio across the inertial range (not necessarily equal to unity), the dynamics can then be shown to be compatible with a variety of inertial range scalings including K41, IK, and WT [8]. Weak MHD turbulence has been observed in the magnetosphere of Jupiter [11], where the strong Jovian field creates a favorable environment for wave interactions to dominate the dynamics. In the solar wind, data for a long time have indicated that the spectrum appears Kolmogorovian [19], although recent observations indicate a more complex dynamics (discussed further in the conclusion).

Numerical simulations to date are unable to give a definitive answer to the question of spectral index in the large (MHD) scales of plasma turbulence, at least in three dimensions. The difference between the K41 and IK scalings is subtle enough that any type of contamination, in particular by intermittency as well as dissipative small-scale effects, will blur the results. Intermittency, the sporadic occurrence of intense small-scale structures, tends to steepen the direct cascade energy spectrum. In fact, it has been shown both in two and three spatial dimensions that intermittency in MHD generally leads to stronger corrections to high-order structure functions than in neutral fluids [14,20,21] and that the magnetic field is more intermittent than the velocity [20,22].

Recent studies indicate that, in the presence of an external force with a given autocorrelation time and/or a strong, uniform magnetic field, the energy spectrum can exhibit different power laws (e.g., [15,23,24]). Such varied spectral indices can be ascribed to the variation of time scales [13] or to the presence of complex structures, such as ribbons (see [15] and references therein and also [25]). However, the possibly simpler problem of incompressible MHD decay in three dimensions with $\mathbf{B}_0 = 0$ has not been examined in this light [26]. Therefore, it is the purpose of this paper to do so by way of high-resolution numerical simulation and to show that indeed several classes of dynamics are possible in decaying MHD turbulence. In the next section, we give equations and initial conditions; Sec. III is dedicated to the temporal behavior of the flows, Sec. IV to the spectra observed in this paper and convergence of the results with Reynolds number, and Sec. V to a discussion and brief concluding remarks.

II. THREE CLASSES OF MAGNETIC TAYLOR-GREEN FLOW

The MHD equations for an incompressible flow with a velocity $\mathbf{v}$ and magnetic induction $\mathbf{b}$ (in units of Alfvén velocity) read

$$\frac{\partial \mathbf{v}}{\partial t} + \mathbf{v} \cdot \nabla \mathbf{v} = -\nabla p + \mathbf{j} \times \mathbf{b} + \nu \Delta \mathbf{v}, \quad (1)$$

$$\frac{\partial \mathbf{b}}{\partial t} = \nabla \times (\mathbf{v} \times \mathbf{b}) + \eta \Delta \mathbf{b},$$

$$\nabla \cdot \mathbf{v} = 0 = \nabla \cdot \mathbf{b}, \quad (2)$$

with p the fluid pressure and $\mathbf{j} = \nabla \times \mathbf{b}$ the current density. In the absence of viscosity ν and resistivity η, the total energy $E^T = \langle \mathbf{v}^2 + \mathbf{b}^2 \rangle / 2 = E^V + E^M$, cross helicity $H^C = \langle \mathbf{v} \cdot \mathbf{b} \rangle / 2$, and magnetic helicity $H^M = \langle \mathbf{a} \cdot \mathbf{b} \rangle / 2$ (where $\mathbf{b} \equiv \nabla \times \mathbf{a}$ defines the magnetic potential, $\mathbf{a}$) are conserved. The Reynolds number here is defined as $\mathrm{Re} = v_{rms} L^T / \nu$, with the integral scale and kinetic and magnetic integral scales defined, respectively, as

$$L^{V,M,T} = 2\pi \frac{\int E^{V,M,T}(k)k^{-1}dk}{\int E^{V,M,T}(k)dk}.$$

Similarly, one can define Taylor Reynolds numbers $R_\lambda^{V,M,T} = v_{rms} \lambda^{V,M,T} / \nu$, where the Taylor scales $\lambda^{V,M,T}$ are defined as

$$\lambda^{V,M,T} = 2\pi \left(\frac{\int E^{V,M,T}(k)dk}{\int E^{V,M,T}(k)k^2 dk} \right)^{1/2}.$$

Ideal MHD ($\nu = 0$, $\eta = 0$) has been studied numerically both in two dimensions [28] and in three [29,30], including with adaptive mesh refinement [31]. Such simulations are important for understanding the initial nonlinear exchanges among modes until the smallest resolved scales are reached, at which point dissipation must be introduced to continue the computation and reach a fully developed turbulent flow with current and vorticity sheets. We are interested here in this subsequent turbulent decay.

The velocity field we choose for our initial conditions is the Taylor-Green (hereafter, "TG") vortex [32] corresponding to a von Kármán flow between two counter-rotating disks. The simplest TG velocity field can be written as [33] (see also [34])

$$\mathbf{v}_{\mathrm{TG}}(x,y,z) = v_0[\sin x \cos y \cos z \hat{\mathbf{e}}_{\mathbf{x}} - \cos x \sin y \cos z \hat{\mathbf{e}}_{\mathbf{y}}].$$

The velocity component in the third direction is zero initially but grows with time. We also define $\boldsymbol{\omega}_{\mathrm{TG}} = \nabla \times \mathbf{v}_{\mathrm{TG}}$ (and $\boldsymbol{\omega} = \nabla \times \mathbf{v}$, the vorticity as usual). This TG vortex has been used not only in numerical studies [35], but also extensively in laboratory studies of fluid turbulence and as a driver for the generation of magnetic fields within flows in liquid metals [36].

A generalization of the TG vortex symmetries to MHD was presented in [30], where the ideal case was studied with the following initial magnetic field configuration:

$$b_x^I = b_0^I \cos(x)\sin(y)\sin(z), \quad (3)$$

$$b_y^I = b_0^I \sin(x)\cos(y)\sin(z), \quad (4)$$

$$b_z^I = -2b_0^I \sin(x)\sin(y)\cos(z). \quad (5)$$

It can be shown that the magnetic field $\mathbf{b}^I$ (which is 2π periodic in the three dimensions) is everywhere perpendicular to the faces, or "walls," of a subvolume defined as $[0, \pi]^3$. The current $\mathbf{j}^I = \nabla \times \mathbf{b}^I$ is then found to be parallel to the walls, which thus can be considered as electrical insulators; for this reason, we refer to this type of TG flow as "insulating." Also of interest is that the global velocity–magnetic field correlation H^C is identically zero and $\mathbf{b}^I = -[b_0/v_0]\boldsymbol{\omega}_{\mathrm{TG}}$.

Another initial condition for the magnetic field was proposed in [30], namely,

$$b_x^C = b_0^C \sin(2x)\cos(2y)\cos(2z), \quad (6)$$

$$b_y^C = b_0^C \cos(2x)\sin(2y)\cos(2z), \quad (7)$$

$$b_z^C = -2b_0^C \cos(2x)\cos(2y)\sin(2z), \quad (8)$$

where the current in the $[0, \pi]^3$ box here is perpendicular to the walls, which are therefore "conducting." In this configuration, H^C is nonzero but weak (less than 4% at its maximum over time in a dimensionless measure relative to the total energy).

TABLE I. Parameters of the runs. N is the equivalent grid resolution; v_{rms} and b_{rms} are the rms velocity and magnetic field at peak of dissipation; ν is the kinematic viscosity and Re the Reynolds number. Note the growth of b_{rms} with Re in all but one case, as well as the decreasing of b_{rms}/v_{rms} going from I to A to C flows. Note that I3 has also been run without imposed symmetries, for comparison purposes.

Run	N	v_{rms}	ν	b_{rms}	Re
I1	128	0.27	2×10^{-3}	0.58	250
I2	256	0.27	1×10^{-3}	0.60	490
I3	512	0.27	5×10^{-4}	0.62	940
I4	512	0.27	2.5×10^{-4}	0.63	1800
I5	1024	0.27	1.25×10^{-4}	0.63	3400
I6	2048	0.32	6.25×10^{-5}	0.59	9700
A1	64	0.39	2×10^{-3}	0.43	260
A2	128	0.38	1×10^{-3}	0.46	460
A3	256	0.37	5×10^{-4}	0.46	780
A4	512	0.37	2.5×10^{-4}	0.47	1500
A5	1024	0.37	1.25×10^{-4}	0.48	2900
A6	2048	0.37	6.25×10^{-5}	0.49	5600
C1	64	0.49	2×10^{-3}	0.31	460
C2	128	0.47	1×10^{-3}	0.32	810
C3	256	0.46	5×10^{-4}	0.34	1500
C4	512	0.46	2.5×10^{-4}	0.37	2700
C5	1024	0.46	1.25×10^{-4}	0.39	4900
C6	2048	0.45	6.25×10^{-5}	0.40	9100

Finally, we also introduce an alternative to the insulating magnetic induction above, which we call $\mathbf{b}^A$ (for "alternative" insulating flow), defined as

$$b_x^A = b_0^A \cos(2x)\sin(2y)\sin(2z), \tag{9}$$

$$b_y^A = -b_0^A \sin(2x)\cos(2y)\sin(2z), \tag{10}$$

$$b_z^A = 0, \tag{11}$$

configuration for which again $H_C = 0$. Note that the magnetic helicity is zero in all three configurations.

All flows are initialized at the largest scales in order to obtain the highest possible Reynolds number and all have unit magnetic Prandtl number (i.e., $\nu = \eta$). The values of the parameters for all runs described in this paper are given in Table I. For the three classes of flow proposed here (named hereafter "I," "A," and "C," referring to the three induction configurations), the same TG velocity is applied at $t=0$ and the fields are normalized such that $E^V(t=0)=E^M(t=0) =0.125$: at the start of each simulation, the kinetic and magnetic energies are in equipartition. The resolutions of the runs range from 64^3 to 2048^3 points (in terms of equivalent grids for computations that would not exploit the flow symmetries; see [30]), allowing the range of Reynolds number to vary over a factor close to 40.

Taylor-Green configurations possess several inherent symmetries (or antisymmetries) within a cube of length 2π (periodicity): mirror (anti)symmetries about the planes $x=0$, $x=\pi$, $y=0$, $y=\pi$, $z=0$, and $z=\pi$; and rotational (anti)symmetries of angle $N\pi$ about the axes $(x,y,z)=(\frac{\pi}{2},y,\frac{\pi}{2})$ and

$(x,\frac{\pi}{2},\frac{\pi}{2})$ and of angle $N\pi/2$ about the axis $(\frac{\pi}{2},\frac{\pi}{2},z)$, for $N \in \mathbb{Z}$. All flows are defined in the $[0,2\pi]^3$ box and satisfy periodic boundary conditions of the domain. Within the domain, the planes of mirror symmetry mentioned above form the insulating and conducting walls of the smaller $[0,\pi]^3$ boxes.

As the symmetries of the TG flows are also symmetries of the MHD equations, they are preserved by time evolution of the solutions. Numerical implementation of the symmetries allows for substantial savings in both computing time and memory usage at a given Reynolds number, with no approximation or closure scheme needed. The numerical method is pseudospectral, with minimum wave number $k_{min}=1$ and maximum wave number $k_{max}=N/3$, where N the number of grid points in each direction, using a 2/3-deliasing rule; the temporal integration is performed using a second-order Runge-Kutta scheme. The code is parallelized using message passing interface (MPI) [37] (see [33] for a detailed implementation for Navier-Stokes and [30] for MHD). It was checked for runs at a resolution of 512^3 grid points (run I3) that the differences between results obtained with the code implementing all the symmetries and those with a general code (in which the symmetries are not imposed explicitly, but the initial conditions are the same) were small and did not grow in time. We have checked that the relative difference for the domain-integrated total enstrophy Ω^T, defined as $\langle \omega^2 + j^2 \rangle / 2$, is of the order of 10^{-5} throughout the computation (see also [30]); it should also be noted that this discrepancy is of the order of the time discretization error of the pseudospectral code itself at this resolution. Further results concerning such a comparison, as well as an analysis of the
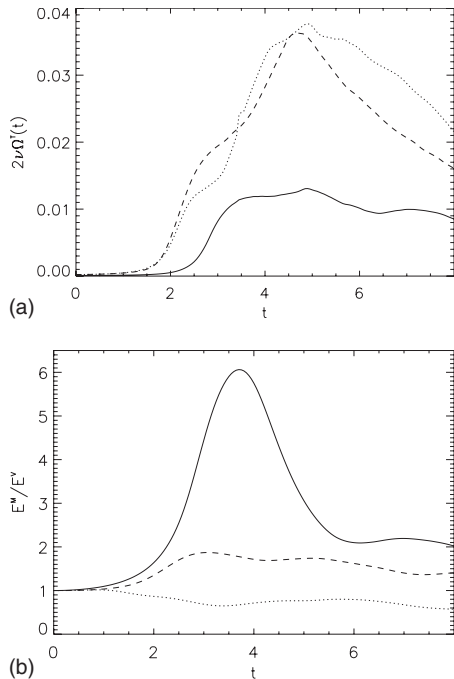
FIG. 1. (a) Temporal evolution of the total dissipation for the highest Reynolds number for each type of flow, represented by runs I6 (solid), A6 (dashed), and C6 (dotted), as described in Table I. (b) Ratio of total magnetic to kinetic energy E^M/E^V for these same runs. Note that I6 has noticeably less dissipation and more magnetic energy.

overall dynamics of the I6 flow, are given in [17].

III. EMERGENCE OF DIFFERENT REGIMES

A. Temporal behavior

As progressively smaller scales become excited, the volume-integrated vorticity and current density grow until dissipation sets in, as can be seen in Fig. 1(a) for the highest-resolution runs I6 (solid line), A6 (dashed line), and C6 (dotted line), following the nomenclature of Table I. The total level of dissipation is substantially lower for run I6.

The energy exchanges between the velocity and magnetic fields yield ratios of magnetic to kinetic energy that change both in time and from flow to flow [Fig. 1(b)]. These differences can also be understood in terms of the diversity of nonlinear terms in the MHD equations, their relative importance depending on the initial conditions. For example, runs I are dominated by magnetic energy after a short period of time, although the initial fields are in equipartition. For this flow, the magnetic field and the vorticity are initially parallel at every point in space. As a result, the nonlinear terms in the MHD equations initially lead to a more rapid production of magnetic energy than in the other flows. At later times, the action of the Lorentz force differentiates the evolution of the magnetic field from that of the vorticity. We find thus that the intrinsic dynamics for the three sets of initial conditions lead to a magnetically dominated flow (I), quasiequipartitioned flow (A), or a flow with subdominant magnetic energy in the large scales (C).
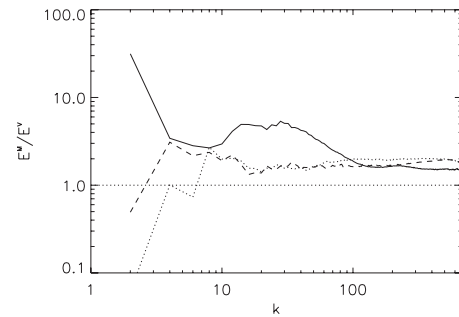

FIG. 2. Ratio of magnetic- to kinetic-energy spectra averaged over $\Delta t = 0.5$ (1.5–2 turnover times) about the maximum of dissipation for run I6 (solid), A6 (dashed), and C6 (dotted); same labels as in Fig. 1. Note the dominance of the magnetic energy at large scale for run I6 and the tendency toward equipartition at small scales for all runs, with a slight excess of magnetic energy.

B. Spectral behavior

The variation with wave number of the ratio of the magnetic- to kinetic-energy spectra for the three high-resolution runs is given in Fig. 2, one for each class. A surplus of magnetic energy at large scale for the I flow is evident as is a tendency in all flows toward quasiequipartition at small scales. A slight excess of small-scale magnetic excitation can be observed, a feature perhaps linked to the absence of a magnetically induced "eddy viscosity" for the magnetic energy akin to one for the kinetic energy, as shown in studies of MHD turbulence using transport coefficients derived from a two-point closure [38].

When examining now the energy spectra, averaged over an interval of time $\Delta t = 0.5$ about the maximum of dissipation of each flow, one can easily distinguish the three flows, with measurably different power laws. Figure 3 (top) gives the total-energy spectra for the three runs, compensated by $k^{5/3}$, calculated from data averaged over 11 temporal outputs at $t \in [3.75, 4.25]$ for I6, $t \in [4.5, 5.0]$ for A6, and $t \in [4.75, 5.25]$ for C6. The A6 flow is near the K41 scaling; the C6 flow has a shallower spectrum close to the IK dynamics, with a $k^{-3/2}$ index, and the I6 flow has a steeper spectrum close to the WT expectation, with a k^{-2} power law (see also Sec. IV). The denotations of the spectra as K41, IK, and WT are used here for simplicity and as will be discussed later, more simulations are needed to decide whether these are the dynamical attractors of the equations or if other solutions exist. Regardless, the three sets of initial conditions clearly lead naturally to different spectral behavior, which can be linked to the several time scales involved in the system as shown next. We recall that in [14], the IK spectrum was followed for larger wave numbers by a steeper spectrum, $k_\perp^{-2}$ corresponding to WT. The data in the present study are not quite sufficient to confirm this finding, but it is possible that the IK spectrum in C6 (dotted line in Fig. 3) is followed by a steeper behavior, with a transition occurring, as in [14], at the magnetic Taylor scale, indicated by an arrow, whereas no such transition is visible for the other two classes of runs, A and I.

In Fig. 3 (bottom), shown is the ratio of the nonlinear eddy time to the Alfvén time, $R_\tau(k) = \tau_e(k)/\tau_A(k)$, where these times are defined as
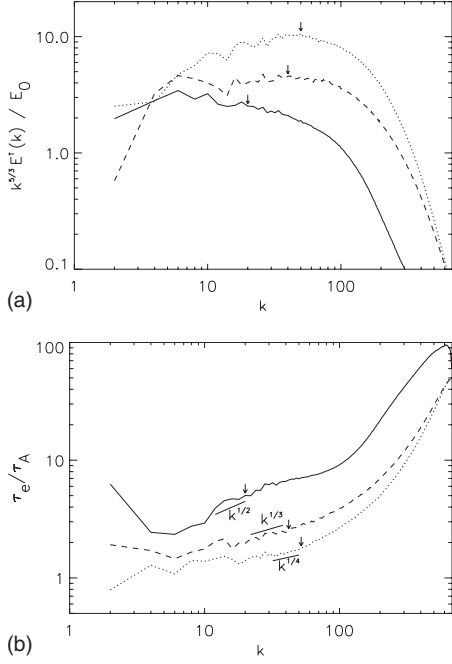
FIG. 3. Total energy spectra (a) compensated by $k^{5/3}$ and averaged over $\Delta t = 0.5$ (1.5–2 turnover times) about the maximum of dissipation and ratio of nonlinear to Alfvén time scales as a function of wave number (b) for the same runs (labels as in Fig. 1: solid line for I, dash for A, and dots for C). Slopes are given only as a reference. The three arrows indicate the magnetic Taylor scale. Note that the three spectra follow noticeably different spectral laws and possibly different scale dependence for their time scales as well (see text).

$$\tau_e(k) = \frac{1}{\sqrt{2k^3 E^V(k)}}, \quad \tau_A(k) = \frac{1}{kB_0},$$

with B_0 the field in the largest-scale mode; hence,

$$R_\tau(k) = \frac{B_0}{\sqrt{2kE^V(k)}}.$$

Contrasting the plots in Fig. 3, we may conjecture that it is the competition between the two characteristic phenomena in MHD turbulence (nonlinear steepening as measured by τ_e^{-1} and wave interactions as measured by τ_A^{-1}) that produces different equilibria among scales and therefore different energy spectra. The fact that these ratios here are always greater than unity is not significant in itself, as phenomenological determination of characteristic times leaves them within some constant factor of order unity, but what may be significant is their variation from flow to flow, as well as their variation with scale.

C. Competition between different phenomena in MHD turbulence

It has been hypothesized that MHD turbulence dynamics may be understood in the context of an equilibrium between turbulent eddies and Alfvén wave interactions [2,5,8,18]. Indeed, the nonlinear MHD equations accept the solutions **v**
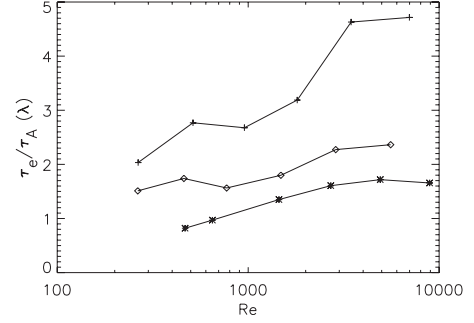

FIG. 4. Variation with Reynolds number Re of the ratio of eddy turnover to Alfvén time scales computed at the Taylor scale λ^M for each flow. I1–I6 (+), A1–A6 ($\diamond$), and C1–C6 ($\ast$) are plotted in order of resolution and Reynolds number, as listed in Table I. All quantities are computed in an interval of $\Delta t = 0.5$ about the peak of dissipation for each run. Note the rather different values of these ratios and onset of saturation for the highest Re indicative of the beginning of a convergence to a high-Re regime.

$= \pm$ **b**. MHD turbulence can also be viewed as the competition between nonlinear steepening and (semi-) dispersive effects, somewhat akin to soliton dynamics [23]. The nonlinear competition between eddies and waves, in this light, could be measured by R_τ. With $R_\tau \approx 1$ at all scales, a K41-type spectrum can occur; relaxing the condition by leaving R_τ equal to any constant, independent of scale, models can be devised [18] to be compatible with the IK phenomenology and WT theory as well [8].

It could be argued that the hypothesis of constancy of R_τ across scales is approximately verified by the data displayed in Fig. 3. However, given τ_e as defined above, R_τ must vary as $k^{1/4}$, $k^{1/3}$, and $k^{1/2}$, respectively, for IK, K41, and WT dynamics. The results shown in Fig. 3 are in fact compatible with this interpretation, although the comparative steepening of $R_\tau(k)$ is subtle.

IV. SCALING WITH REYNOLDS NUMBER

A. Do global features of the TG flows vary with Reynolds number?

It is notoriously difficult to measure spectral indices of power laws found in numerical simulations, in particular, because of the small extent of the inertial range, sandwiched in wave number space between the energy-containing and dissipative scales. To address this issue, we now turn to a convergence study of the data.

Figure 4 shows how the ratio R_τ, evaluated at the magnetic Taylor scale λ^M, changes with Reynolds number for each class of run. We see that it tends toward a constant whose value depends on the type of flow, although higher Reynolds numbers should be investigated to confirm this tendency. While the fully converged values may not be present in our study, a transition toward convergence of R_τ appears to take place at Re $\approx 3 \times 10^3$ after a long evolution over a sequence of smaller Reynolds numbers. For this reason, simulations at moderate Reynolds numbers can only hint at asymptotic results needed to understand fully developed turbulence.
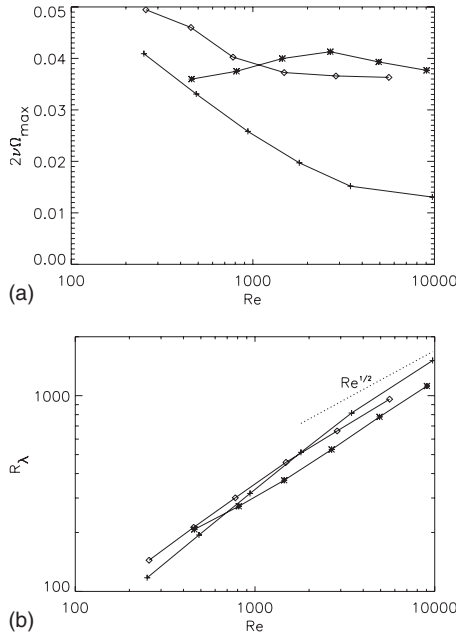
FIG. 5. Scaling as a function of Reynolds number Re of the maximum value of the dissipation over time (a) and of the Taylor Reynolds number R_λ computed at the instantaneous peak of dissipation (b); straight line indicates the turbulent scaling $R_\lambda \sim \mathrm{Re}^{1/2}$. Symbols are as in Fig. 4.

Other indicators can be examined to further suggest convergence, at least for the highest two resolutions (runs 5 and 6) for each class of flow. In Fig. 5 we show—again as a function of Reynolds number—the variation of the maximum of dissipation (top) and the Taylor Reynolds number (bottom). We observe that the maximum of dissipation for the A and C initial conditions tends to level off toward a constant value as the Reynolds number is increased, as seen before in two-dimensional MHD [39,40], three-dimensional Navier-Stokes [41], and an earlier three-dimensional MHD study [42]. The I flows seem to show a different trend; we observe a slowing of its decrease and in fact the trend follows a power-law when examining the first maximum (as opposed to the absolute maximum, at $t \approx 3.25$ and ≈ 4.75, respectively, see Fig. 1(a), and [17]). It should nevertheless be noted that, for each class, the maximum of dissipation occurs at a time that depends significantly on the Reynolds number (not shown). Finally, we observe a clear scaling of the Taylor Reynolds number R_λ [43] with the large-scale Reynolds number Re [Fig. 5(b)]: the two flows at the highest Reynolds numbers for each class are consistent with $R_\lambda \sim \mathrm{Re}^{1/2}$, indicating again an asymptotic trend.

B. Evolution of spectra with Reynolds number

With reasonable evidence of convergence of flows beyond a Reynolds number threshold, we can now turn to the energy spectra we observe. Figure 6 displays, for each class of initial conditions, the total-energy spectra averaged again over an interval $\Delta t = 0.5$ (approximately 1.5–2 eddy-turnover times) about the maximum of dissipation of each run. The spectra are compensated by k^2 for the I flows, by $k^{5/3}$ for the A flows,
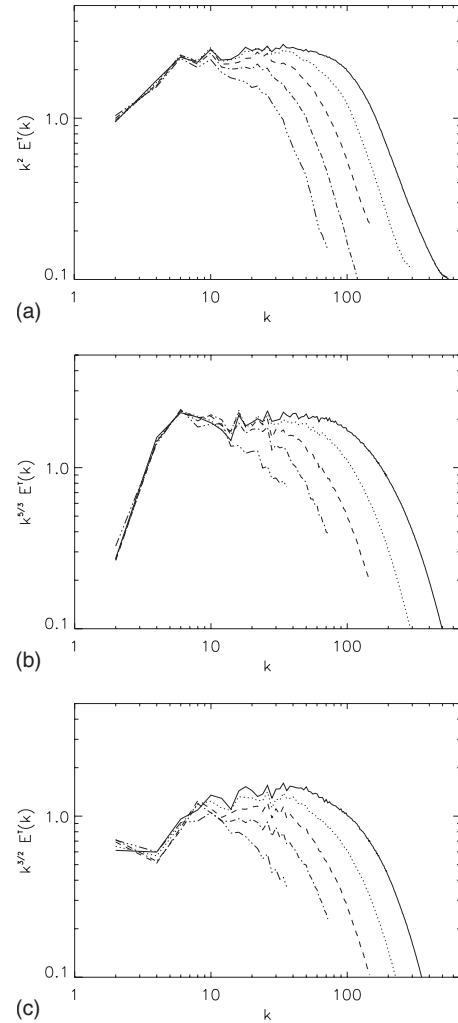

FIG. 6. Total energy spectra averaged over $\Delta t = 0.5$ (1.5–2 turn-over times) around the time of maximum dissipation for different Reynolds numbers for the following flows (see Table I): I runs compensated by k^2 (a), A runs compensated by $k^{5/3}$ (b), and C runs compensated by $k^{3/2}$ (c). Dash-triple dots, dash-dots, dashes, dots, and solid lines represent, respectively, the runs I2–I6, A2–A6, and C2–C6. Equivalent resolutions range from 128^3 to 2048^3 grid points.

and by $k^{3/2}$ for the C flows. These plots strongly suggest that the scaling predictions of WT, K41, and IK give credible descriptions of the I, A, and C flows, respectively, recognizing that intermittency can steepen the spectrum of the self-similar solutions. We note also that for C6, the $k^{-3/2}$ scaling seems to end at the magnetic Taylor scale ($\lambda^M \sim 0.13$), beyond which bending of magnetic field lines is felt and a steeper power law is possible, as already found in [14], but no such double power law is observed for the other two classes of flow. Furthermore, a bottleneck at the beginning of the dissipation range is noticeably absent or undetectable, likely due to the intrinsic nonlocality of nonlinear interactions in MHD [44].

The observed differences in spectra in these particular simulations are linked to the different initial conditions, but in a more general sense they are also correlated with the ratio for time scales, which are only implicitly prescribed by the
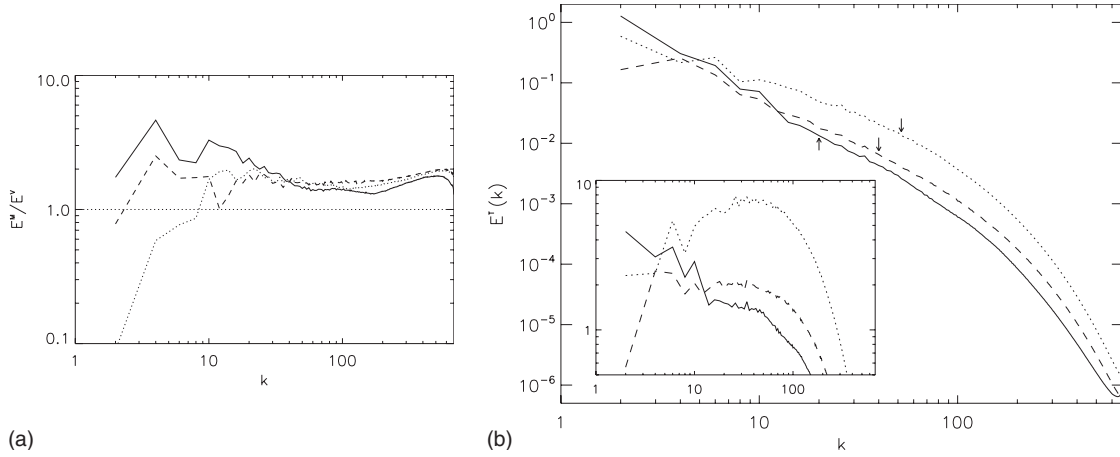
FIG. 7. (a) Magnetic- to kinetic-energy ratio as a function of wave number at late time ($t \in [6, 6.5]$) and averaged over $\Delta t = 0.5$. Again, we plot I6 (solid), A6 (dashed), and C6 (dotted). Note that the excess of magnetic energy at low wave number in I6 has subsided to 1/15 of its former value. (b) Total energy spectra for the same runs over the same time interval. Arrows indicate the new magnetic Taylor wave number for each run. In the insert, the same spectra are compensated by $k^{3/2}$. Note the similar energy ratios and inertial range scaling for the three flows.

initial conditions, as already discussed and displayed in Fig. 3. This finding is further confirmed by the following analysis. It is clear in Fig. 1 (*bottom*) that at late time ($t \gtrsim 5.5$), the ratio of magnetic to kinetic energy does not differ as much for the three types of flows studied in this paper. We thus examine in Fig. 7 the ratio of magnetic- to kinetic-energy spectra (a) and the energy spectra (b) averaged over $\Delta t = 0.5$, as before, but now at a later time, beginning averaging at $t = 6$. Indeed, when the kinetic and magnetic energies are comparable, the energy spectra of the I and A flows likewise have comparable spectral index, the C flow (dotted line) being somewhat shallower at this late time, and with a Reynolds number that is lower than in the I case. However, the I flow is clearly not as steep as at earlier times; we conclude that, for a given initial condition, different spectra may occur at different times.

V. DISCUSSION AND CONCLUSION

In order to show that different energy spectra emerge in decaying MHD turbulence in the absence of a uniform magnetic field, we have generalized the Taylor-Green flow to MHD and studied three different configurations, which, from a statistical point of view, are *a priori* equivalent since they have the same invariants (E^T, H^C, and H^M) and the same equipartition of kinetic and magnetic energies at initial time. By taking advantage of the symmetries of these flows, we have been able to examine higher Reynolds numbers than in a full direct numerical simulation at a given cost. The symmetries also helped to expedite a convergence study in terms of Reynolds number, attaining $R_\lambda \sim 960$ or above in all three flows at the highest resolution. We found that the I class behaves somewhat differently than the other two, with slower dissipation of energy and a lower maximum of dissipation at a given Reynolds number. We also discovered that the three flows dynamically partition kinetic and magnetic energies differently at large scales, likely the source of their different spectral behavior.

There is a wealth of theoretical, phenomenological, observational, and numerical studies of energy spectra for MHD turbulence. Solar wind data seemed for a long while to favor the K41 classical spectrum, but a puzzling recent result is that, in some cases, both IK- and K41-type power laws have been observed for the velocity and magnetic field [12]. Moreover, recent data on MHD turbulence in the plasma sheet using the CLUSTER suite of satellites indicate that the inertial index in this environment may vary but with more likelihood for a k^{-2} law and to a lesser extent a $k^{-1.6}$ power law for the energy spectrum [45]. The tendency toward K41 or IK dynamics has also been observed recently in several numerical simulations [13,15,23] with different forcing functions (see also [46]). In fact, it has been shown numerically for the reduced MHD equations [5] that a whole palette of spectra is possible [23,24].

The different power laws observed in our study can in principle be associated with known "solutions" (K41, IK, or WT) of MHD turbulence (omitting intermittency corrections) and they are found to be correlated with the ratio of the nonlinear to the Alfvén time. This is linked to the competition between nonlinear steepening and dispersion due to waves, which can interact as they propagate forward and backward along a mean field. Whether or not there are other attractors for MHD remains to be determined. It is conceivable that multiple fixed points can coexist, linked with K41 (fluidlike), IK (balance between steepening and dispersion), and WT (turbulence and waves) dynamics. For example, one numerical study, though performed at low resolution, showed that on long-time scales, multiple attractive solutions are indeed possible for decaying incompressible MHD in the absence of an imposed magnetic field: one dominated by the velocity, another dominated by the magnetic field, and the third with quasiequipartition between the two modes of energy [47]. Are the solutions we observe in our study, which build up on short-time scales (of the order of the eddy-turnover time), associated with the various long-time asymptotic states of decaying MHD? This hypothesis might

be tested by analyzing simulations at very long times for the different TG MHD flows described here and variants thereof, a task left for future work.

The work presented in this paper can be extended in many directions. For example, one might consider the effect of the presence or absence of correlations between the velocity and the magnetic field or the influence of the degree of intermittency of the flow. Further work should also include exploring runs at higher Reynolds numbers. Short of waiting for the next generation of resources (which will be made available, e.g., through the petascale computing initiative), one can resort to modeling methods, in addition to direct numerical simulation. Akin to the one presented here, insofar as implementing a reduction of modes at a given Reynolds number, is the numerical algorithm that decimates modes (somewhat arbitrarily) in the dissipation range [48]. Another possibility is the use of large-eddy simulations that compare well against high-resolution direct numerical simulations, such as in [49]. Of a different nature is the Lagrangian averaging approach, or alpha model, which can be viewed as a sort of direct numerical simulation methodology imposing a filter to the small scales by means of a closure consistent with preserving the Hamiltonian nature of the flow, although these averaged equations conserve the ideal invariants using a different norm than $\mathcal{L}_2$ [50]. With alpha models (see, e.g., [51]), it has recently been shown that the result found in [14] of a double inertial range in MHD, of isotropic IK followed (spectrally) by a weak turbulence spectrum, can be recovered at substantially lower cost. Using a combination of such modeling tools may allow for parametric investigations of MHD turbulence and thereby lead to a better understanding of such flows as they occur in geospace, the heliosphere, and the interstellar medium, as well as of their influence on cosmic-ray propagation or solar-terrestrial interactions.

[1] A. N. Kolmogorov, Dokl. Akad. Nauk. SSSR **30**, 9 (1941); **32**, 16 (1941); Proc. R. Soc. London, Ser. A **434**, 9 (1991); **434**, 15 (1991).

[2] P. Iroshnikov, Astron. Zh. **40**, 742 (1963); R. H. Kraichnan, Phys. Fluids **8**, 1385 (1965).

[3] B. Lehnert, Q. Appl. Math. **12**, 321 (1955).

[4] A. Alemany, R. Moreau, P.-L. Sulem, and U. Frisch, J. Mech. **18**, 277 (1979); M. Garnier, A. Alemany, P.-L. Sulem, and A. Pouquet, J. Mec. **20**, 233 (1981).

[5] H. R. Strauss, Phys. Fluids **19**, 134 (1976).

[6] D. Montgomery and L. Turner, Phys. Fluids **24**, 825 (1981); P. Veltri, A. Mangeney, and M. Dobrowolny, Nuovo Cimento B **68**, 235 (1982); J. Shebalin, W. H. Matthaeus, and D. Montgomery, J. Plasma Phys. **29**, 525 (1983).

[7] V. Carbone and P. Veltri, Geophys. Astrophys. Fluid Dyn. **52**, 153 (1990); S. Oughton, E. R. Priest, and W. H. Matthaeus, J. Fluid Mech. **280**, 95 (1994); P. Goldreich and S. Sridhar, Astrophys. J. **485**, 680 (1997); C. S. Ng and A. Bhattacharjee, Phys. Plasmas **4**, 605 (1997); R. M. Kinney and J. C. McWilliams, J. Plasma Phys. **57**, 73 (1997); Phys. Rev. E **57**, 7111 (1998).

[8] S. Galtier, A. Pouquet, and A. Mangeney, Phys. Plasmas **12**, 092310 (2005).

[9] S. Boldyrev, Phys. Rev. Lett. **96**, 115002 (2006).

[10] S. Galtier, S. V. Nazarenko, A. C. Newell, and A. Pouquet, J. Plasma Phys. **63**, 447 (2000); Astrophys. J. **564**, L49 (2002).

[11] J. Saur, H. Politano, A. Pouquet, and W. H. Matthaeus, Astron. Astrophys. **386**, 699 (2002).

[12] J. J. Podesta, D. A. Roberts, and M. L. Goldstein, Astrophys. J. **664**, 543 (2007).

[13] W.-C. Müller and R. Grappin, Phys. Rev. Lett. **95**, 114502 (2005).

[14] P. D. Mininni and A. Pouquet, Phys. Rev. Lett. **99**, 254502 (2007).

[15] J. Mason, F. Cattaneo, and S. Boldyrev, Phys. Rev. E **77**, 036403 (2008).

[16] J. Perez and S. Boldyrev, Astrophys. J. **672**, L61 (2008).

[17] A. Pouquet, E. Lee, M. E. Brachet, P. D. Mininni, and D. Rosenberg, Geophys. Astrophys. Fluid Dyn. (to be published); e-print arXiv:0906.4860.

[18] P. Goldreich and S. Sridhar, Astrophys. J. **438**, 763 (1995).

[19] W. H. Matthaeus and M. L. Goldstein, J. Geophys. Res. **87**, 6011 (1982).

[20] H. Politano, A. Pouquet, and V. Carbone, Europhys. Lett. **43**, 516 (1998).

[21] L. Sorriso-Valvo, V. Carbone, P. Veltri, H. Politano, and A. Pouquet, Europhys. Lett. **51**, 520 (2000).

[22] P. D. Mininni and A. Pouquet, Phys. Rev. E **80**, 025401 (2009).

[23] P. Dmitruk, D. O. Gómez, and W. H. Matthaeus, Phys. Plasmas **10**, 3584 (2003).

[24] A. F. Rappazzo, M. Velli, G. Einaudi, and R. B. Dahlburg, Astrophys. J. **657**, L47 (2007).

[25] B. Bigot, S. Galtier, and H. Politano, Phys. Rev. E **78**, 066301 (2008).

[26] In two space dimensions, the slower decay of MHD turbulence, compared to Navier-Stokes flows, has been studied both with a model and with direct numerical simulations (see [27]).

[27] S. Galtier, H. Politano, and A. Pouquet, Phys. Rev. Lett. **79**, 2807 (1997); S. Galtier, E. Zienicke, H. Politano, and A. Pouquet, J. Plasma Phys. **61**, 507 (1999).

[28] U. Frisch, A. Pouquet, P.-L. Sulem, and M. Meneguzzi, J. Mec. Theor. Appl. **2**, 191 (1983).

[29] R. M. Kerr and A. Brandenburg, Phys. Rev. Lett. **83**, 1155

(1999).

[30] E. Lee, M. E. Brachet, A. Pouquet, P. D. Mininni, and D. Rosenberg, Phys. Rev. E **78**, 066401 (2008).

[31] R. Grauer and C. Marliani, Phys. Rev. Lett. **84**, 4850 (2000).

[32] G. I. Taylor and A. E. Green, Proc. R. Soc. London, Ser. A **158**, 499 (1937).

[33] M. E. Brachet, D. I. Meiron, S. A. Orszag, B. G. Nickel, R. H. Morf, and U. Frisch, J. Fluid Mech. **130**, 411 (1983).

[34] M. E. Brachet, C. R. Acad Sci., Ser. II: Mec., Phys., Chim., Sci. Terre Univers **311**, 775 (1990); Fluid Dyn. Res. **8**, 1 (1991).

[35] C. Nore, M. E. Brachet, H. Politano, and A. Pouquet, Phys. Plasmas **4**, 1 (1997); Y. Ponty, P. D. Mininni, D. C. Montgomery, J. F. Pinton, H. Politano, and A. Pouquet, Phys. Rev. Lett. **94**, 164502 (2005); New J. Phys. **9**, 296 (2007); Y. Ponty, J. P. Laval, B. Dubrulle, F. Daviaud, and J. F. Pinton, Phys. Rev. Lett. **99**, 224501 (2007); C. R. Acad. Sci. (Paris) **9**, 749 (2008).

[36] M. Bourgoin et al., Phys. Fluids **14**, 3046 (2002).

[37] D. O. Gómez, P. D. Mininni, and P. Dmitruk, Adv. Space Res. **35**, 899 (2005); Phys. Scr., T **116**, 123 (2005).

[38] A. Pouquet, U. Frisch, and J. Léorat, J. Fluid Mech. **77**, 321 (1976).

[39] D. Biskamp and H. Welter, Phys. Fluids B **1**, 1964 (1989).

[40] H. Politano, A. Pouquet, and P.-L. Sulem, Phys. Fluids B **1**, 2330 (1989).

[41] Y. Kaneda et al., Phys. Fluids **15**, L21 (2003); P. D. Mininni, A. Alexakis, and A. Pouquet, Phys. Rev. E **77**, 036306 (2008).

[42] P. D. Mininni, A. G. Pouquet, and D. C. Montgomery, Phys. Rev. Lett. **97**, 244503 (2006).

[43] The Taylor Reynolds number, whose given value is computed at the peak of dissipation, saturates from that time onward.

[44] A. Alexakis, P. D. Mininni, and A. Pouquet, Phys. Rev. E **72**, 046301 (2005); J. Pietarila Graham, P. D. Mininni, and A. Pouquet, ibid. **80**, 016313 (2009).

[45] J. M. Weygand et al., J. Geophys. Res. **110**, A01205 (2005).

[46] K. Yoshida and T. Arimitsu, Phys. Fluids **19**, 045106 (2007).

[47] T. Stribling and W. H. Matthaeus, Phys. Fluids B **2**, 1979 (1990).

[48] M. Meneguzzi, H. Politano, A. Pouquet, and M. Zolver, J. Comput. Phys. **123**, 32 (1996).

[49] J. Baerenzung, H. Politano, Y. Ponty, and A. Pouquet, Phys. Rev. E **77**, 046303 (2008); **78**, 026310 (2008).

[50] D. D. Holm, Chaos **12**, 518 (2002).

[51] J. P. Graham, P. D. Mininni, and A. Pouquet, Phys. Rev. E **72**, 045301(R) (2005); J. Pietarila Graham, D. D. Holm, P. D. Mininni, and A. Pouquet, Phys. Fluids **18**, 045106 (2006).